YYU JINAS, Volume 31, 373-392, 2026 https://doi.org/10.53433/yyufbed.18315749

Yuzuncu Yil University Journal of the Institute of Natural & Applied Sciences

https://dergipark.org.tr/en/pub/yyufbed

Research Article

Behavior of Low-Strength Concrete Confined by High-Strength Composite Layer under Axial Loading

Zeynep UTMA[*1], **Emre AKIN**[1*], **İsmet VAPUR**[1]

[1]Mersin Üniversitesi, Mühendislik Fakültesi, İnşaat Mühendisliği Bölümü, Mersin, Türkiye
*Corresponding author e-mail: 22023330017@mersin.edu.tr

Abstract: This study investigates the behavior under axial loading of low-strength concrete under a composite confinement layer consisting of fiber-reinforced high-strength mortar and a reinforcement mesh (geogrid). Within the scope of the experimental program, low-strength (10-15 MPa) cylindrical concrete specimens with dimensions of 150x300 mm were confined using high-strength mortar containing 2% steel or polypropylene fibers and geogrids with varying numbers of layers. Axial compression tests were conducted at the Mersin University laboratory using a 3000 kN capacity computer-controlled concrete testing machine, and the data were recorded using a TDS-530 data acquisition unit. To ensure that the confinement layer provided only a passive confinement effect, an axial load was applied directly to the core concrete using specialized steel plates. The critical parameters investigated included the thickness of the high-strength mortar (15 and 25 mm), fiber type, reinforcement mesh type, and number of layers. The effects of these parameters on the axial strength, energy dissipation capacity, and lateral deformations were systematically evaluated. The results demonstrated that the proposed confinement technique significantly enhanced the strength and deformation capacity (ductility) of low-strength concrete. It was determined that a thicker mortar layer (25 mm) primarily increased the strength, whereas an increased number of reinforcement mesh layers contributed more significantly to the ductility. Furthermore, the findings revealed that the use of polypropylene fibers generally yielded better results in terms of strength and ductility than steel fibers and effectively limited the crack widths.

Keywords: Strengthening, Confinement, Concrete, Axial load behavior, Fiber-reinforced, Mesh reinforcement.

Yüksek Dayanımlı Kompozit Tabakayla Sargılanan Düşük Dayanımlı Betonun Eksenel Yük Altındaki Davranışı

Özet: Bu çalışma, düşük dayanımlı betonun eksenel yük davranışını; lif takviyeli yüksek dayanımlı harç ve donatı ağı (geogrid) içeren kompozit bir sargılama tabakası altında incelemektedir. Deneysel program kapsamında, 150x300 mm boyutlarındaki düşük dayanımlı (10-15 MPa) silindirik beton numuneler; %2 oranında çelik veya polipropilen lif içeren yüksek dayanımlı harç ve farklı katman sayılarındaki geogridler ile sargılanmıştır. Eksenel basınç testleri, Mersin Üniversitesi laboratuvarında 3000 kN kapasiteli bilgisayar kontrollü beton presi altında, TDS-530 veri toplama ünitesi kullanılarak gerçekleştirilmiştir. Sargı tabakasının sadece pasif çevreleme etkisi oluşturması için yük, özel çelik plakalar aracılığıyla doğrudan çekirdek betona uygulanmıştır. İncelenen kritik parametreler arasında yüksek dayanımlı harç kalınlığı (15 mm ve 25 mm), kullanılan lif türü, donatı ağı türü ve katman sayısı bulunmaktadır. Bu parametrelerin eksenel dayanım, enerji sönümleme kapasitesi ve yanal deformasyonlar üzerindeki etkileri sistematik olarak değerlendirilmiştir. Sonuçlar, önerilen sargılama tekniğinin düşük dayanımlı betonun hem dayanımını hem de şekil değiştirme kapasitesini (sünekliğini) önemli ölçüde artırdığını göstermiştir. Kalın harç tabakasının (25 mm) öncelikli olarak dayanımı yükselttiği, artan donatı ağı katman sayısının ise sünekliğe daha fazla katkı sağladığı belirlenmiştir. Ayrıca, polipropilen lif kullanımının dayanım ve süneklik açısından çoğunlukla çelik life göre daha iyi sonuçlar verdiği ve çatlak genişliklerini sınırladığı gözlenmiştir.

Anahtar Kelimeler: Güçlendirme, Sargılama, Beton, Eksenel yük davranışı, Lif takviyeli, Hasır donatı.

Received Date:29.11.2025
Accepted Date: 19.07.2026

How to cited: Utma Z, Akın E, Vapur İ. (2026). Behavior of Low-Strength Concrete Confined by High-Strength Composite Layer under Axial Loading. *Yuzuncu Yil University Journal of the Institute of Natural and Applied Sciences, 31,* 373-392. https://doi.org/10.53433/yyufbed.1831549

1. Introduction

In the highly active seismic zones throughout the world, there exists a substantial building stock characterized by significant deficiencies and irregularities stemming from design, construction, and in-service usage (Üzümeri et al., 1999; Ersoy & Özcebe, 2000; Özcebe et al., 2004; Ersoy, 2009). A considerable portion of these structures lack adequate supervision during construction. Consequently, these buildings often exhibit insufficient strengths and ductilities. Currently, most existing reinforced concrete structures contain concrete with compressive strengths typically ranging from 8 to 16 MPa, which falls short of fulfilling the requirements stipulated by contemporary seismic codes (Arslan & Korkmaz, 2007). This underscores the presence of numerous existing structures across the country that possess inadequate resistance to seismic events. Addressing this critical issue primarily involves the demolition and subsequent reconstruction of seismically vulnerable structures (Gündoğay, 2022). However, seismic rehabilitation becomes a more convenient solution when long-term disuse of the structure cannot be tolerated or the costs of seismic rehabilitation are much lower. The seismic rehabilitation of structures against earthquake effects can be at the level of system improvement and/or element strengthening, depending on the results of performance analyses. Element strengthening can be applied to various structural components (columns, beams, shear walls, beam-column joints, etc.) to resist different force conditions (axial, shear, flexural, or torsional) based on the specific needs of the structure. Column jacketing is one such element strengthening method for improving the axial response of columns. The selection of the technique for column jacketing largely depends on the choice of material used for strengthening the column. In the past, reinforced concrete jacketing was a widely preferred technique, primarily because of its cost-effectiveness and the greater experience of strengthening firms with concrete-based solutions.

In contrast, the fiber-reinforced polymer (FRP) strengthening technique, offered as an alternative to column jacketing, is considered relatively new compared to other strengthening methods. Synthetic fiber-reinforced polymer (FRP) composites, which include organic epoxy resins as the matrix material, exhibit superior mechanical properties, rendering them highly effective and user-friendly in contemporary construction applications. Their utility extends to the seismic rehabilitation of existing deficient structural elements and their integration into novel structural designs. A prominent application of these advanced composites in the retrofitting of substandard buildings involves the confinement of columns to augment their axial performance characteristics (Mirmiran & Shahawy, 1997; Lam & Teng, 2003; Berthet et al., 2005; Mandal et al., 2005; Lam et al., 2006; Ozbakkaloglu & Oehlers, 2008; Ozcan et al., 2010; Ozbakkaloglu & Akin, 2012; Wei & Wu, 2012; Carrillo & Valencia-Mina, 2020; Gündoğay, 2024). Nevertheless, a notable drawback associated with FRPs is the substantial energy consumption and concomitant carbon dioxide emissions during their manufacturing processes, which contribute to significant environmental concerns (Ku & Wang, 2011). In addition to their relatively high cost, the deterioration of mechanical properties under high temperature, irreversibility, and toxicity lead to additional disadvantages. To overcome these deficiencies, new column confinement methods have emerged that are based on the use of thin inorganic cement-based matrices and high-strength fibers in the form of mesh fabrics (i.e., fiber-reinforced cementitious matrix, FRCM). Although an enhancement in the axial response can be achieved using this method, most studies have reported that this enhancement lags behind the improvement in the axial load behavior supplied by FRP confinement (Trapko, 2013; Colajanni et al., 2014; Cascardi et al., 2017; Ombres & Mazzuca, 2017).In the last decade, the confinement of concrete using high-performance mortar or concrete, including short fibers, has emerged as an alternative to FRP or FRCM confinement. The thickness applied in this method (15–40 mm) is larger than that in the FRCM method. Few studies in the literature have concluded that the ultimate compressive strength and strain capacity can be enhanced by the applied confinement (Tian et al., 2020; Zeng & Long, 2022).

This study aimed to investigate the improvement in the axial load behavior of low-strength concrete through confinement with a composite layer. This composite layer is specifically reinforced with a relatively thick high-strength fiber-reinforced concrete (FRC) and polyester-based mesh reinforcement. The parameters under investigation included the thickness of the high-strength concrete layer, type of fiber incorporated within this layer, and both the number of layers and position of the mesh reinforcement. The primary objectives of this study were to determine the contributions of various arrangements of fiber-reinforced high-strength concrete and mesh reinforcement in enhancing the behavior under axial loading of concrete and to comparatively analyze the changes induced by these individual parameters on the behavior under axial loading. For this purpose, key performance indicators, such as axial strength, ductility, and lateral deformation characteristics, were evaluated to characterize the behavior under axial loading.

2. Experimental Program

2.1. Materials

In this study, two distinct types of polyester-based uniaxial geogrid mesh reinforcements were utilized within the confinement layer. These geogrids, knitted from high-tenacity polyester yarns, feature a manufacturer-specified ultimate tensile strength of 150 kN/m. To enhance durability against environmental factors, particularly the alkaline media of the concrete and temperature fluctuations, the second group of geogrids was treated with a protective polymeric coating. Beyond the coating, these geogrids exhibit dimensional variations: the uncoated type has 25 mm × 30 mm apertures with rib thicknesses of 10 mm and 5 mm, whereas the coated type features 20 mm × 20 mm apertures with rib thicknesses of 5 mm and 3 mm.

Regarding fiber reinforcement, micro straight steel fibers and fibrillated polypropylene fibers were incorporated into the high-strength mortar mixtures. Both fiber types were added at an equal weight-based dosage. However, it is explicitly acknowledged that due to the significant density disparity between the materials (7850 kg/m^3 for steel vs. 910 kg/m^3 for polypropylene), this constant weight dosage results in substantially different fiber volume fractions (V_f). Additionally, two different types of fibers, steel and polypropylene, were incorporated into the high-strength concrete layer, mixed at 2% by weight. Consequently, the comparative performance of these fibers should be interpreted as an evaluation at a constant weight-based dosage rather than a direct comparison at equal volumes. The comprehensive physical and mechanical properties of all reinforcement materials are summarized in Table 1.

Table 1. Physical and mechanical properties of the reinforcement materials

Type of Material	Material Detail	Density (kg/m^3)	Tensile Strength	Dimensions / Aperture (mm)	Fiber Content
Fibers	Steel Fiber	7850	>2000 MPa	l:13, d:0.2	2.0%
	Polypropylene Fiber	910	400−600 MPa	l:12, d:0.05	2.0%
Geogrids	Uncoated Geogrid	-	150 kN/m	25×30 (Rib:10x5)	-
	Coated Geogrid	-	150 kN/m	20×20 (Rib: 5x3)	-

To accurately capture the deformation characteristics of the specimens, axial and lateral strain developments were meticulously monitored using high-precision electrical resistance strain gauges. These gauges were specifically engineered for cementitious materials, featuring a longer base to account for the heterogeneous nature of concrete and mortar. Prior to the installation, the application surfaces were carefully prepared by grinding and cleaning to ensure a monolithic bond between the gauge and the confinement layer. The gauges were positioned at the mid-height of the cylinders to mitigate the influence of end-restraint effects. All strain data, alongside the axial load, were synchronized and recorded at a constant frequency using a high-speed TDS-530 data acquisition system, ensuring a continuous capture of the stress-strain relationship until the post-peak failure stage. The detailed technical specifications, including the gauge factor, resistance, and dimensions of the strain gauges, are summarized in Table 2.

2.2. Test specimens

A total number of 19 low-strength concrete cylinders having a diameter of 150 mm and a height of 300 mm were prepared and tested under monotonic axial compression. The specimens were prepared using mix proportions typical of poor concrete, aiming to represent the concrete of substandard buildings (Table 3). The curing period was 28 days. One reference specimen was a bare concrete cylinder, whereas the other specimens were strengthened by wrapping them with high-strength composite layers.

Table 2. Technical properties of strain gauge

Type of Strain Gauge	PL-60-11-3LJC-F	**Lot No**	P217712
Gauge Length	60 mm	**Quantity**	10
Gauge Factor	2.1±1%	**Test Condition**	23°C 50%RH
Gauge Resistance	120±0.5 Ω	**Batch No**	WC29U
Lead Wires		10/0.12 2W 3m r=0.32(Ω/m)	

Table 3. Concrete mix proportions

Type of Concrete	**Mass Ratios (%)**						
	Fine aggregate	Coarse aggregate	Cement	Water	Fiber	Superplasticizer	Total
Low-Strength Core Concrete	19	58	12	11	-	-	100
High-Strength Concrete	34	36	20	7.5	2	0.5	100

Two thicknesses (15 and 25 mm) were used for the high-strength concrete layer. The target strength for the high-strength concrete with the mix proportions shown in Table 3 was aimed as 50-55 MPa. The resulting average 28-day compressive strength of the high-strength concrete was 51 MPa.

For the strengthening process, cylindrical molds were placed around pre-prepared low-strength core concrete to achieve the desired layer thickness. The mesh reinforcement, shaped into cylinders, was positioned at two different locations with varying numbers of layers according to the experimental design. Following the placement of the mesh reinforcement, fiber-reinforced high-strength concrete was cast into the annular space between the low-strength core and outer mold. To ensure proper consolidation and eliminate voids, rodding and a vibration table were employed during the casting process. All specimens were demolded at the joints one day after casting. Subsequently, the specimens strengthened with fiber-reinforced high-strength concrete were submerged in a curing tank for 28 days to achieve their design strength. Figure 1 illustrates the sequential strengthening stages performed using high-strength concrete.

Both ends of the cylindrical specimens were capped using a high-strength repair mortar with a specified 28-day compressive strength of 60 MPa. The aim of capping was to provide flat surfaces to enable uniform axial load distribution during the tests. After the capping of the specimens was completed, the attachment of strain gauges, which are part of the test setup to measure lateral strains, began one day before the compression test was conducted. Two lateral strain gauges were used on each specimen strengthened with a high-strength composite layer. The strain gauges on the cylindrical specimens were positioned 180° apart from each other. Care was also taken to vertically center the strain gauges. After determining the location of the strain gauge, the area of the surface was cleaned with pure alcohol to remove dust and create a smooth surface. Super glue was applied to the surface of the strain gauge that would contact the specimen, and it was affixed to the designated location (Figure 2).

2.3. Specimen designation

The reference is designated as "REF". In the confined specimen designations, "T" represents the thickness of the confinement layer, followed by a specific thickness value. Two different thickness values were used: 15 and 25 mm. Next, the type of fiber within the high-strength concrete is indicated by "D" for steel fiber or "F" for polypropylene fiber. Subsequently, "G" denotes whether an additional mesh reinforcement is present. The number “2” follows this if there are two layers of mesh reinforcement. If a single layer of mesh reinforcement is used, no number is added after the mesh reinforcement designation. The final part indicates the position of the mesh reinforcement within the confining layer: "M" for the middle and "E" for the end, where it interfaces with the core concrete. For example, "T25D-G2M" describes a specimen confined with a composite layer of high-strength concrete containing steel fibers with a thickness of 25 mm, reinforced with two layers of mesh reinforcement located in the middle of this thickness. The details and designations of the specimens are presented in Table 4.

Figure 1. Preparation of the concrete specimens

Figure 2. The strain gauge attached to the specimen

Table 4. Details of the specimens

Group	Layer thickness (mm)	Type of fiber	Position and number of mesh reinforcement layers
REF	-	-	-
T15D-GM	15	Steel	Single layer in the middle
T15F-GM		Polypropylene	Single layer in the middle
T25D	25	Steel	-
T25F		Polypropylene	-
T25D-GM		Steel	Single layer in the middle
T25F-GM		Polypropylene	Single layer in the middle
T25F-G2M		Polypropylene	Two layers in the middle
T25F-GMGE		Polypropylene	Single layer in the middle + single layer at the end

2.4. Test setup and instrumentation

The experiments were conducted at the Mersin University Civil Engineering Laboratory using a 3000 kN capacity standard concrete compression testing machine. Monotonic axial loading was applied to each specimen. During the tests of the wrapped specimens, a 10 mm thick circular steel plate made of high-strength oven-baked steel with the same diameter as the core concrete was placed between the top surface of the test machine and the specimen. In the experiments, this plate was positioned directly over the core concrete to ensure that the axial load was applied only to the core concrete. This procedure was carried out based on the assumption that in the confinement practice, no axial load would be transferred to the confining layer, and only radial stresses from the expanding concrete would be present in the confinement. During the tests, the vertical (axial) displacements were measured using three potentiometers with a 100 mm range. The data from the potentiometers were acquired and recorded using a data acquisition system (DAS) during the test. A cable connected to the press of the compression testing machine enabled the real-time acquisition of the applied load. In addition, the lateral strains on the confining layer were measured using two strain gauges with a capacity of 60 mm. Axial compression loads were applied to all specimens at a rate of 4 kN/s for the entire test duration. Figure 3 shows the axial compression test setup.

3. Test Results

3.1. Failure modes

The typical failure modes of the confined concrete specimens after testing are shown in Figure 4. During the tests, the specimens generally did not exhibit brittle behavior, and cracks remained at the capillary level until they approached compressive strength. In some specimens, the crack widths did not increase significantly even after reaching the peak strength. However, the tests were concluded because of widening cracks at more advanced stages under increasing vertical displacements. Upon examining the specimens after the tests, it was generally observed that the crack widths formed near the top and bottom platen regions were greater than those in the middle section (Figure 4).

Specimens T25F-GM and T25F-GMGE completed the compression test, forming only capillary cracks. Generally, the number of cracks in the 25 mm thick specimens (typically a single notable crack) was slightly less than that in the 15 mm thick specimens. Similarly, it can generally be observed that the post-test damage in the specimens containing polypropylene fibers within the high-strength concrete layer was less compared to those containing steel fibers (Figure 4).

Figure 3. The axial compression test setup

3.2. Axial stress-strain response

The axial compressive stresses and strains were calculated from the experimental load and displacement data using Eq. (1) and Eq. (2), respectively. For each sample, an axial stress-strain graph was plotted, and the average compressive strength and post-elastic deformation capacity were calculated.

$$\sigma = P/A \tag{1}$$
$$\varepsilon = (\Delta l)/l \tag{2}$$

In these equations, σ is the axial compressive stress, ε is the axial strain, P is the applied compressive load, A is the cross-sectional area of the confined core concrete, Δl is the axial displacement (i.e., shortening), and l is the initial height of the specimens (i.e., 300 mm). The ultimate compressive strength of the specimens was determined for the reference (f_{co}) and confined specimens (f_{cc}) and presented in Table 4. The ultimate values of all specimens (ε_{cu}) are also listed in the same table to provide insight into their deformability. Additionally, the energy dissipation capacities of the specimens (E_{diss}) were obtained as the area under the σ-ε curves up to the failure point of the specimens (i.e., the modulus of toughness) and are presented in Table 4.

The average and maximum values of the strength increments in each group with respect to the reference specimen (f_{cc}/f_{co}) are listed in Table 4. In addition, the average and maximum increases in the energy dissipation capacity of the confined specimens ($E_{diss,conf.}$) in each group with respect to the reference ($E_{diss,ref.}$) are presented in this table ($E_{diss,conf.}/E_{diss,ref.}$). In the evaluations of each test group, the maximum increment was highlighted only if the difference between the average and maximum values of strength and energy dissipation was significant for the individual specimens of the test group. Otherwise (when the average and maximum values were close), the evaluation was based solely on the average value.

The stress–strain diagrams of the T15D-GM specimens confined by a single mesh reinforcement layer within a 15 mm thick mortar containing steel fibers are presented in Figure 5. a. On average, the two T15D-GM specimens achieved a compressive strength of 15.45 MPa, improving the reference strength by an average factor of 1.17. Notably, specimen T15D-GM-1 exhibited a significantly higher strength of 20.32 MPa, representing a 1.53-fold increase over the reference. In terms of energy dissipation capacity, the T15D-GM group specimens collectively showed an average

2.52-fold enhancement relative to the reference. The highest E_{diss} increase within this group, reaching 3.54-fold, was attributable to the specimen T15D-GM-1 (Table 5).

Figure 4. The failure modes of the specimens in different test groups

The average compressive strength of the specimens in the T15D-GM group was 15.46 MPa, representing a 1.17-fold increase over the reference specimen (Table 5). Additionally, the average energy dissipation enhancement ratio ($E_{diss/conf.}/E_{diss/ref.}$) was calculated as 2.52. The compressive strength of specimen T15D-GM-2 was lower than expected and even lower than the reference value. This may be partly attributed to local damage sustained during the demolding process. Despite being restored with high-strength structural repair mortar, this specimen was retained in the experimental program to evaluate the influence of such localized defects on the overall confinement performance and to provide a comprehensive comparative analysis.

The average compressive strength of all three specimens in the T15F-GM group was 15.93 MPa, indicating an average 1.2-fold increase compared to the reference specimen (Table 5). The average enhancement ratio in the energy dissipation capacity ($E_{diss/conf.}/E_{diss/ref.}$) was calculated as 2.04. The specimen group, consisting of a 15 mm thick high-strength concrete layer reinforced with a single layer of geogrid at its mid-depth and containing polypropylene fibers, included three samples. The need for a third specimen arose because the mesh reinforcement, initially intended to be positioned precisely at the center between the core concrete and the mold, shifted during the casting process and failed to maintain its design alignment. Consequently, an additional casting was performed for the third specimen (T15F-GM-3), where the mesh was securely fixed to ensure proper reinforcement of the concrete.

The average compressive strength of the T25D group specimens was 24.13 MPa. This average strength represents an increase of 1.82 times compared to the strength of the reference sample (Table 5). Specifically, for the T25D-1 specimen, this increase ratio was 2.02 times. Furthermore, the average enhancement ratio in the energy dissipation capacity of the T25D group specimens was determined to be 2.16.

The average compressive strength of the T25F group was 26.72 MPa (i.e., more than two times the strength of the reference). On the other hand, the average enhancement ratio of the energy dissipation capacity was 4.94. However, it should also be noted that the energy dissipation capacity of specimen T25F-1 increased by 5.81-fold compared to that of the reference. The average compressive strength of the two specimens in the T25D-GM group was 19.54 MPa, which corresponds to 1.47 times increase compared to the reference specimen. As a result of the strengthening applied to this group, the average enhancement ratio of the energy dissipation capacity was calculated as 3.03.

Table 5. Test results

Group	Specimen	f_{co} or f_{cc} (MPa)	Avg. f_{cc}/f_{co}	Max. f_{cc}/f_{co}	ε_{cu}	E_{diss} (MJ/m^3)	Avg. $E_{diss,conf}$./ $E_{diss,ref.}$	Max. $E_{diss,conf}$./ $E_{diss,ref.}$	$\varepsilon_{ult,lat.}$ (%)
REF	REF-AVG	13.25	-	-	0.0047	0.048	-		-
T15D-GM	T15D-GM-1	20.32	1.17	1.53	0.0107	0.170	2.52	3.54	0.226
	T15D-GM-2	10.6			0.0089	0.072			0.006
T15F-GM	T15F-GM-1	15.24	1.20	1.28	0.007	0.089	2.04	2.67	0.068
	T15F-GM-2	15.62			0.0097	0.128			0.451
	T15F-GM-3	16.93			0.0057	0.077			1.063
T25D	T25D-1	26.7	1.82	2.02	0.0049	0.099	2.16	2.25	0.054
	T25D-2	21.55			0.0070	0.108			0.014
T25F	T25F-1	28.53	2.02	2.15	0.0117	0.279	4.94	5.81	0.487
	T25F-2	24.9			0.0112	0.195			0.680
T25D-GM	T25D-GM-1	17.11	1.47	1.66	0.0104	0.115	3.03	3.67	0.010
	T25D-GM-2	21.96			0.0100	0.176			0.065
T25F-GM	T25F-GM-1	28.64	2.42	2.67	0.0050	0.110	2.21	2.29	0.610
	T25F-GM-2	35.41			0.0042	0.102			0.390
T25F-G2M	T25F-G2M-1	25.45	1.82	1.92	0.0094	0.197	4.71	5.31	0.627
	T25F-G2M-2	22.9			0.0150	0.255			0.133
T25F-GMGE	T25F-GMGE-1	23.17	1.96	2.69	0.0050	0.082	3.98	6.65	0.057
	T25F-GMGE-2	19.25			0.0114	0.172			0.335
	T25F-GMGE-3	35.6			0.0107	0.319			-

In the T25F-GM group, the average compressive strength of the specimens was 32.03 MPa (i.e., 2.42 times the increment in strength with respect to the reference). The energy dissipation capacity was enhanced by an average ratio of 2.21 in this group.

The average compressive strength of the two specimens in the T25F-G2M group was 24.18 MPa. This strengthening intervention increased the average strength by 1.82 times that of the reference specimen. The specimens of the T25F-G2M group experienced an enhancement of 4.71-fold on average with respect to the reference in terms of energy dissipation capacity.

The tests were terminated when the load-carrying capacity dropped to 85% of the peak load, as the specimens continued to deform. The energy dissipation capacity values were also calculated up to the same ultimate data point.

During the casting of T25F-GMGE-1 and -2, which were wrapped with two layers of geogrid (one central and one at the end), difficulties were encountered, leading to poor concrete compaction and necessitating repair with honeycomb defects on the concrete surface. The same high-strength repair mortar used for capping the specimens was also utilized for the repair (i.e., filling of the honeycomb defects). Consequently, a third specimen for this group, T25F-GMGE-3, was prepared more carefully with better compaction, which did not require repair. The experimental results showed that while the average compressive strength of specimens T25F-GMGE-1 and T25F-GMGE-2 was 21.21 MPa, the compressive strength of specimen T25F-GMGE-3 was 35.60 MPa (Figure 5.h). Furthermore, the experimental data indicated that the average enhancement ratio of the energy dissipation capacity of all three specimens in the T25F-GMGE group was 3.98. As a result of the care in the quality of the confinement of T25F-GMGE-3, a 6.65-fold average improvement was achieved in the energy dissipation capacity compared to that of the reference in this group.

3.3. Lateral strains

The ultimate lateral strain values ($\varepsilon_{ult,lat}$) obtained from the strain gauges during the tests of all the specimens are provided in the last column of Table 5. It should be noted that the strain values could not be obtained from the DAS owing to technical problems in the case of specimen T25F-GMGE.

No explicit correlation was observed between the ultimate (rupture) strains ($\varepsilon_{ult,lat}$), presented in Table 5, and the resulting strength and ductility enhancements. The maximum strain values obtained from the strain gauges on different specimens varied significantly, independent of the experimental parameters. Furthermore, even the maximum strain values obtained from the two different strain gauges on the same specimen exhibited substantial variations. For instance, the strain values obtained from the strain gauges (SG1 and SG2) vs. loading step graphs of specimens T15F-GM-3 and T25D-GM-2 are presented in Figure 6.

As shown in Figure 6.a, the ultimate lateral strains experienced by the two strain gauges of specimen T15F-GM-3 were 1.063% and 0.217%. The similar strains measured on specimen T25D-GM-2 were 0.065% and 0.013%, respectively (Figure 6. b). The significant difference between not only the strains of two specimens, but also the two strains of each individual specimen is clear. It was generally observed that in specimens where low ultimate strain values were recorded by the strain gauges, cracks formed away from the strain gauges, while in specimens where relatively higher strain values were measured, the strain gauges were located close to the cracks.

These results are contrary to the results of the axial compression tests of FRP-confined concrete specimens, where there are no such significant discrepancies between the lateral strain values on the circumference of the specimen (Akin et al., 2020). This indicates that until rupture, the strains along the same circumference (on the same circle) in the FRP confinement material exhibit similar magnitudes (i.e., a more uniform distribution). Furthermore, in previous studies, a correlation was observed between the strength and strain enhancements obtained from the axial test results of FRP-confined specimens compared to equivalent unconfined concrete specimens and the measured ultimate strain values, which is reflected in the relevant numerical models. The absence of the same correlation in this study, where a thick concrete layer was used for confinement, can be evaluated based on the aforementioned observations. Based on the experimental observations, it can be concluded that the strains developed in the thick concrete confining layer under radial stresses induced by the expanding core concrete are not as uniform as those in the FRP materials. This finding, which requires further support from additional experimental studies, might be a crucial aspect to consider in models reflecting the behavior of concrete confined with a relatively thick concrete layer.

4. Discussions

The confinement provided by a thick FRC layer with/without additional mesh reinforcement for low-strength concrete (i.e., approximately 10 MPa) considerably increased the axial compressive strength and energy dissipation capacity in all cases, consistent with the findings reported by Ilki et al. (2004) and Rousakis et al. (2007). However, the amount of enhancement depends on the test parameters and the quality of the implementation of confinement, as explained in the following. In general, the axial compressive stress-strain curves have a descending second portion after attaining the ultimate strength at the end of the ascending first portion of the response. There was a smooth transition between these two parts of the response in most specimens, indicating that the specimens lost their rigidity owing to the formation of cracks in the confining concrete and core layers. In contrast to the general trend, there was an ascending second portion in some of the specimens (T25F-1, T25F-2, T25D-GM-2, and T25F-GMGE-3) with varying slopes. Among these specimens, T25F-1 exhibited a strain-hardening behavior at an approximate axial strain level of 0.6%. The slope of the second region was slightly negative up to this strain level. In these specimens with an ascending second portion, failure was indicated by several cracks with a smaller crack width compared to the other specimens that experienced fewer cracks with larger crack widths (Figure 6).

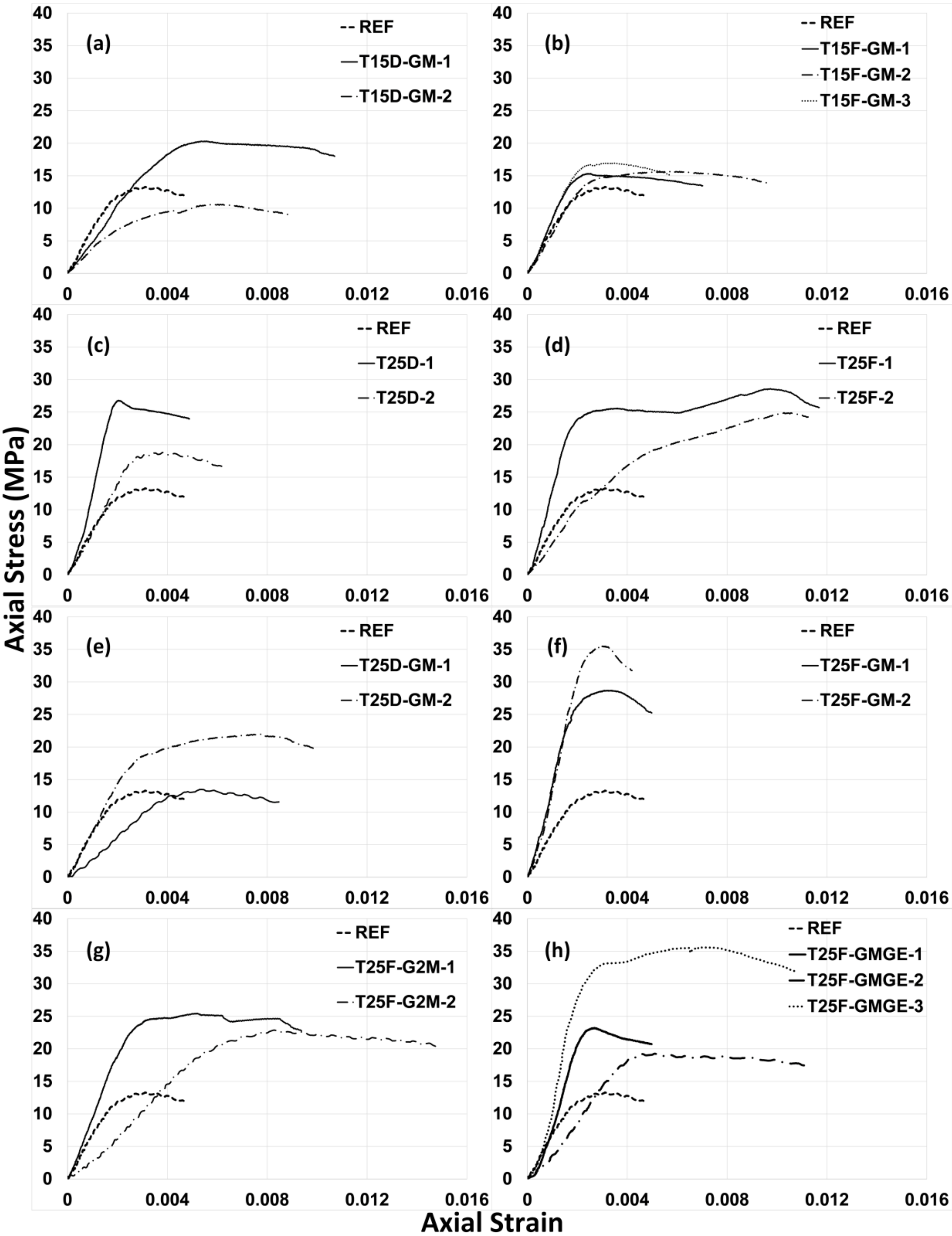

Figure 5. Axial stress-strain diagrams of the test specimens

Based on these observations, it can be stated that the fibers within the concrete provided a redistribution of stresses and a more progressive and widespread damage formation in these specimens. The absence of this situation in other confined specimens may be due to quality issues in the production of the confinement layer, as was visible in the T25F-GMGE group (explained previously). Another reason may be the nonuniform straining of the thick confining concrete layer when subjected to the radial stresses induced by the expanding concrete (as explained in the previous section).

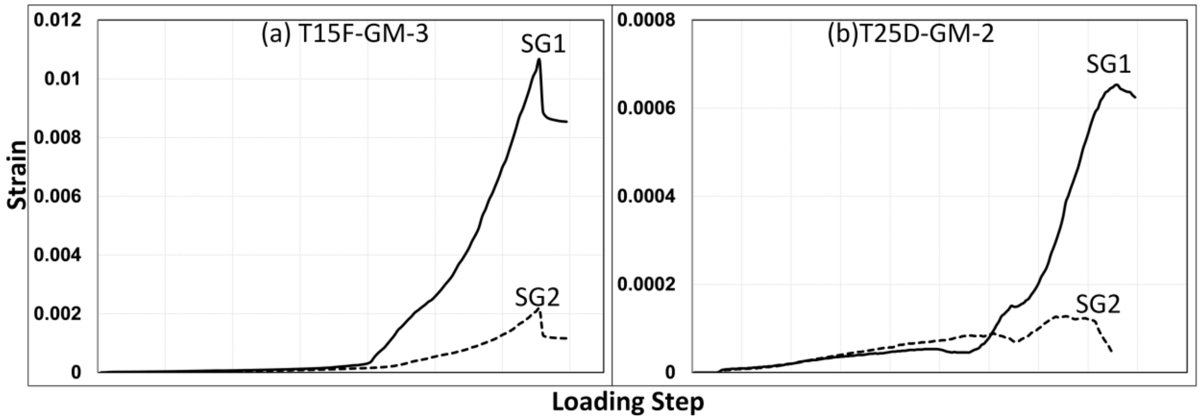

Figure 6. Lateral strain curves of (a) T15-F-GM-3 and (b) T25D-GM-2

A comparison of the experimental results presented in Table 5 reveals a consistent increase in the axial compressive strength (considering both the average and maximum values) as the confining mortar layer thickness increased (e.g., T25D-GM vs. T15D-GM and T25F-GM vs. T15F-GM). Notably, in the groups reinforced with polypropylene fibers, this enhancement ratio reached as high as 100% when comparing T25F-GM to T15F-GM. However, it should be emphasized that while the fiber additions were kept constant by weight, the significant density disparity between the steel and polypropylene fibers resulted in substantially different fiber volume fractions (V_f). Consequently, the observed performance variations, particularly the high enhancement ratios in the polypropylene groups, should be interpreted as a comparison of mixtures with equal weight dosages rather than a pure evaluation of fiber efficiency alone. Furthermore, the results indicate that the substantial gain in compressive strength was not proportionally matched by an increase in energy dissipation capacity as the confinement thickness increased, suggesting a more complex interaction between the mortar thickness and post-peak behavior.

When comparing the specimen groups strengthened with one and two layers of mesh reinforcement (that is, T25F-GM vs. T25F-G2M and T25F-GMGE), it is evident that increasing the number of these reinforcement layers had no positive effect on axial strength enhancement. However, an increase in the number of layers resulted in a significant increase in the energy dissipation capacity (approximately 200%). This indicates that the contribution of mesh reinforcement is more evident in improving post-peak behavior and energy absorption capacity, whereas its effect on axial strength remains less consistent. This result aligns with the findings of Wang et al. (2016), who reported that while polymer mesh reinforcement contributes minimally to axial strength, it significantly enhances the post-peak ductility and deformability of concrete members. Furthermore, it is explicitly acknowledged that the potential influence of specimen preparation quality and manual application of the geogrid layers may have contributed to these observed variations in strength trends. In the test group, T25F-GMGE, the specimen T25F-GMGE-3, which was prepared with better concrete compaction and quality control, provided better results not only compared with the specimens in the same group but also with those in the T25F-G2M group. Except for specimen T25F-GMGE-3, the allocation of the two layers of mesh reinforcement at different levels within the confining concrete did not cause a significant difference in the ultimate strength and energy dissipation capacity.

The experimental study incorporated two types of fibers (steel and polypropylene), each comprising 2% by weight of the mortar layer used for confinement. As the unit weight of the polypropylene fibers was smaller than that of the steel fibers, the volume of the polypropylene fibers was higher within the confining concrete. Steel fibers were exclusively utilized in the T15D-GM, T25D, and T25D-GM groups, all of which had corresponding polypropylene fiber-containing counterparts for comparative analysis. A comparison of the average results from these groups with different fiber types revealed that polypropylene fiber usage generally yielded slightly better outcomes in terms of strength (Table 5). However, there are variable results in terms of energy absorption capacity related to the use of different fibers in confinement. Comparing the specimens in the T15D-GM vs. T15F-GM and T25D-GM vs. T25F-GM groups, the steel fibers resulted in a slightly higher enhancement in the energy dissipation capacity. However, the comparison of the specimens in the T25D and T25F groups provided opposite results, with a much higher difference in the energy dissipation capacities (i.e., superior results of polypropylene with respect to the steel fibers). Furthermore, post-test examination of the specimens revealed that those confined with a polypropylene fiber-reinforced concrete layer generally exhibited smaller (hairline) crack widths than their steel fiber-reinforced counterparts (Figure 4).

Future research on this topic can be expanded by incorporating additional parameters. The weight percentage of the fiber content within the mortar layer could be varied. Additionally, as previously stated, there is potential to explore different concrete properties for the confining layer; a similar study could be conducted using self-consolidating mortars or those with exceptionally high workability. Furthermore, the use of alternative mesh materials instead of geogrids should be investigated.

5. Prediction of the Confinement Effectiveness

In the literature, there are models to predict the ultimate strength (fcu) and strain (εcu) of concrete confined by FRCM or high-performance mortar. These models depend on the experimental results of either FRP or FRCM-confined concrete (Donnini et al., 2019). The models proposed by Triantafillou et al. (2006), De Caso y Basalo et al. (2012) and Ates et al. (2019), which are produced according to the results of FRCM confinement, were used to predict the ultimate strength and/or strain of the specimens tested in this study. These models are summarized in Table 6. It should be noted that the model by De Caso y Basalo et al. (2012) only provides an expression for the prediction of the ultimate strength of confined concrete, but no expression for the ultimate strain.

Table 6. Analytical models to predict the ultimate strength and strain of confined concrete

Model	**Analytical expressions**	
	Ultimate Strength	Ultimate Strain
Triantafillou et al. (2006)	$f_{cc} = f_{co}[1 + 1.90(f_{lu}/f_{co})]$	$\varepsilon_{cu} = \varepsilon_{co} + 0.047(f_{lu}/f_{co})$
De Caso y Basalo et al. (2012)	$f_{cc} = f_{co}[1 + 2.87(f_{lu}/f_{co})^{0.775}]$	-
Ates et al. (2019)	$f_{cc} = f_{co}[1 + 3.67(f_{lu}/f_{co})]$	$\varepsilon_{cu} = 1.35\varepsilon_{co} + 0.026(f_{lu}/f_{co})$

In the expressions given in Table 6, f_{co} is the compressive strength of the unconfined reference specimen (i.e., 13.25 MPa) and ε_{co} is the strain corresponding to the compressive strength of unconfined concrete (i.e. 0.003). f_{lu} is the lateral confining pressure supplied by the confinement, which may be assumed to be the summation of those provided by the high-strength concrete including fibers, $f_{lu,concr.}$. and mesh reinforcement, $f_{lu,\text{ and mesh}}$ (if the latter exists) (Zhao, 2020). The stresses on the confined concrete section are shown in Figure 7. In this figure, r_i is the radius of the core concrete (75 mm), r_o is the outer radius of the confined section (90 mm for the 15 mm confinement and 100 mm for the 25 mm confinement), D is the diameter of the core concrete (150 mm), and t is the thickness of the confinement (15 mm or 25 mm).

The theory of elasticity can be utilized to determine the tangential stresses on the thick-walled confining layer (with thickness "t") under internal pressure caused by the Poisson effect of the compressed core concrete (Popov, 1998). These tangential stresses have a nonlinear distribution, with the highest value at the inner boundary ($\sigma_{t,i}$) and the lowest value at the outer boundary ($\sigma_{t,o}$). The tangential stress, σ_t, at any point between the inner and outer boundaries of the confining layer at a radius of "r" (r_i<r<r_o) may be determined by Eqn. 3, where the internal pressure, pi, can be taken equal to the lateral confining pressure supplied by a high-strength concrete layer ($f_{lu,concr.}$).

$$\sigma_t(r) = \frac{p_i\, r_i^2}{r_o^2 - r_i^2}\left(1 + \frac{r_o^2}{r^2}\right) \tag{3}$$

Here, the nonlinear distribution of tangential stresses is transformed into an equivalent uniform distribution to yield the average tangential stress (σt,avg) for simplicity. This is done by equating the resultants of both the nonlinear and uniform tangential stress distributions (Eqn. 4).

$$\int_{r_i}^{r_o} \sigma_t(r)\, dr = \sigma_{t,avg}(r_o - r_i) \tag{4}$$

By utilizing Eqns. (3) and (4), one may determine the average tangential strain as given in Eqn.(5).

$$\sigma_{t,avg} = \frac{p_i\, r_i}{r_o - r_i} = \frac{f_{lu,concr.}\, r_i}{r_o - r_i} \tag{5}$$

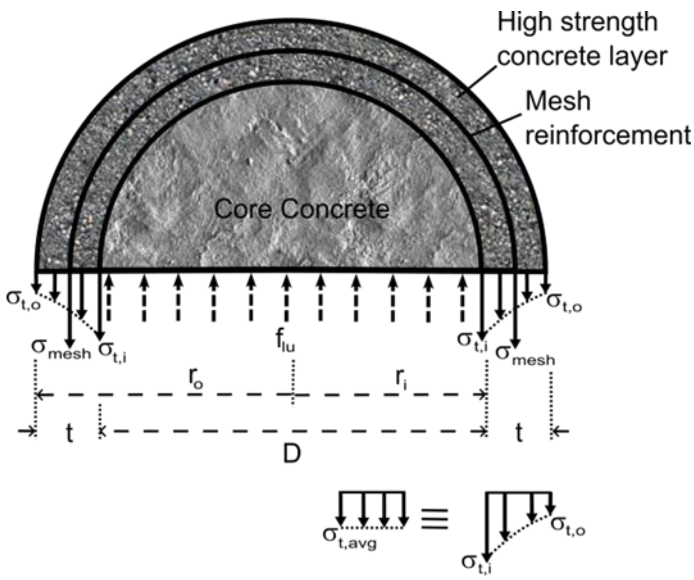

Figure 7. Lateral confining pressure

If $\sigma_{t,avg}$ is equated to the tensile strength of the high-strength confining concrete layer ($f_{ct,conf.}$), then, the contribution of the confining pressure from this layer, $f_{lu,concr.}$ can be estimated. $f_{ct,conf.}$ value can be determined using the expression suggested by Song and Hwang (2004) and given in Eqn. 6 for the splitting tensile strength of the fiber included concrete ($f_{cst,conf.}$). The splitting tensile strength of concrete ($f_{cst,conf.}$) can be transformed into the direct tensile strength ($f_{ct,conf.}$) to be utilized in Eqn. 5 using the expression proposed by Wu et al. (2023), which is given in Eqn. 7.

$$f_{cst,conf.} = 0.63\sqrt{f_{cc,conf.}} + 3.01V_f - 0.02V_f^2 \tag{6}$$

$$f_{ct,conf.} = 1.23 f_{cst,conf.}^{0.5466} \tag{7}$$

In Eqn. 6, $f_{cc,conf.}$ is the compressive strength of the high-strength concrete used for confinement, and V_f (%) is the fiber volume fraction of the concrete. The fiber volume fractions were estimated as 0.23% and 3.2% for the steel and polypropylene fiber-reinforced concrete, respectively. By using Eqn. 6, the splitting tensile strengths of concrete with steel and polypropylene fibers can be calculated as 5.2 MPa and 13.8 MPa, respectively. According to Eqn. 7, the direct tensile strength values of the concrete including steel and polypropylene used for the confinement were 3.0 MPa and 5.2 MPa, respectively. As mentioned previously, the contribution of the high-strength concrete layer with fibers to the lateral confining pressure ($f_{lu,concr.}$) can be determined using Eqn. 5 for confinement thicknesses of 15 and 25 mm separately (where $\sigma_{t,avg}$ equals the direct tensile strength values of the concrete).

In contrast, the contribution of the mesh reinforcement to the confining pressure ($f_{lu,mesh}$) for the specimens with mesh reinforcement can be estimated using the well-known expression for confinement given in Eqn. 8. $f_{t,mesh}$ is the ultimate tensile strength of the mesh reinforcement in Fig.7 (i.e. σ_{mesh} becomes to be $f_{t,mesh}$ at the rupture point of the mesh reinforcement in this figure).

$$f_{lu,mesh} = \frac{2\, f_{t,mesh}\, t}{D + t} \tag{8}$$

As stated before, the tensile strength of the mesh reinforcement per length was provided as equal to 150 kN/m by the manufacturer, which can be taken directly equal to "$f_{t,mesh}.t$" multiplication in Eqn. 8. The resulting lateral confining pressure values are presented in Table 6, considering the different test parameters of this study.

Using the lateral confining pressure values presented in Table 7, the analytical models provided in Table 6 can be employed to predict the ultimate compressive strength and strain of the test groups in this study. These predicted results ($f_{cc,model}$ and $\varepsilon_{cc,model}$) vs. the average experimental results of each test group ($f_{cc,exp.}$ and $\varepsilon_{cc,exp.}$) are shown in Figure 8.

Table 7. The lateral confining pressure values for different test parameters

Confinement thickness, t	**Fiber Type**	**$f_{lu,conc.}$ (MPa)**	**$f_{lu,mesh}$**	**f_{lu} (MPa)**
15 mm	Steel	0.60	1.82	2.42
	Polypropylene	1.04		2.86
25 mm	Steel	1.00	1.71	2.71
	Polypropylene	1.73		3.44

To determine the lateral confining pressure in test group T25F-G2M, $f_{lu,mesh}$ was simply multiplied by "2" to represent the doubled thickness of the two layers of mesh reinforcement, and the corresponding $f_{lu,concr.}$ was added. The test group T25F-GMGE was not included in the comparison. The results shown in Figure 8 are also listed in Table 7.

The mean error (ME), mean absolute error (MAE), root mean square error (RMSE), coefficient of variation (COV) and mean value of the "model prediction (MP)/experimental result (ER)" ratio are listed in Table 9 for the considered models.

The predictions of ultimate strength across all models exhibit significant variability, with no consistent trend of underestimation or overestimation. The ultimate compressive strength predictions by Triantafillou et al. (2006) are generally more conservative.

Table 8. The ultimate experimental results and corresponding model predictions

Test Group	**$f_{cc,exp.}$ (MPa)**	**$f_{cc,model}$ (MPa)**			**$\varepsilon_{cu,exp.}$**	**$\varepsilon_{cu,model}$**	
		Triantafillou	Basalo	Ates		Triantafillou	Ates
T15D-GM	15.46	17.85	23.43	22.13	0.0098	0.0116	0.0088
T15F-GM	15.93	18.68	24.84	23.75	0.0075	0.0131	0.0097
T25D	24.13	15.15	18.38	16.92	0.0060	0.0065	0.0060
T25F	26.72	16.54	21.10	19.60	0.0115	0.0091	0.0074
T25D-GM	19.54	18.40	24.37	23.20	0.0102	0.0126	0.0094
T25F-GM	32.03	19.79	26.62	25.88	0.0046	0.0152	0.0108
T25F-G2M	24.18	25.60	35.15	37.11	0.0122	0.0261	0.0168

However, this model aligns more closely with the experimental ultimate strengths, as indicated by lower error metrics (Table 9), except for three specimens (T25D, T25F, and T25F-GM). Conversely, the models proposed by Triantafillou et al. (2006) and Ates et al. (2019) tend to overestimate the ultimate strain of the test groups. Nonetheless, the ultimate strain predictions by Ates et al. (2019) demonstrate greater consistency with the experimental results, as evidenced by lower error metrics in Table 9.

Table 9. The lateral confining pressure values for different test parameters

Error Metrics	Ultimate Strength, f_{cc}			Ultimate Strain, ε_{cu}	
	Triantafillou	Basalo	Ates	Triantafillou	Ates
ME	-3.709	2.275	1.515	0.0047	0.0010
MAE (MPa)	5.585	7.063	7.364	0.0053	0.0027
RMSE (MPa)	7.077	7.371	7.806	0.0071	0.0034
COV (%)	29.08	30.99	33.06	52.04	45.91
Mean Ratio (MP/ER)	0.885	1.166	1.127	1.646	1.214

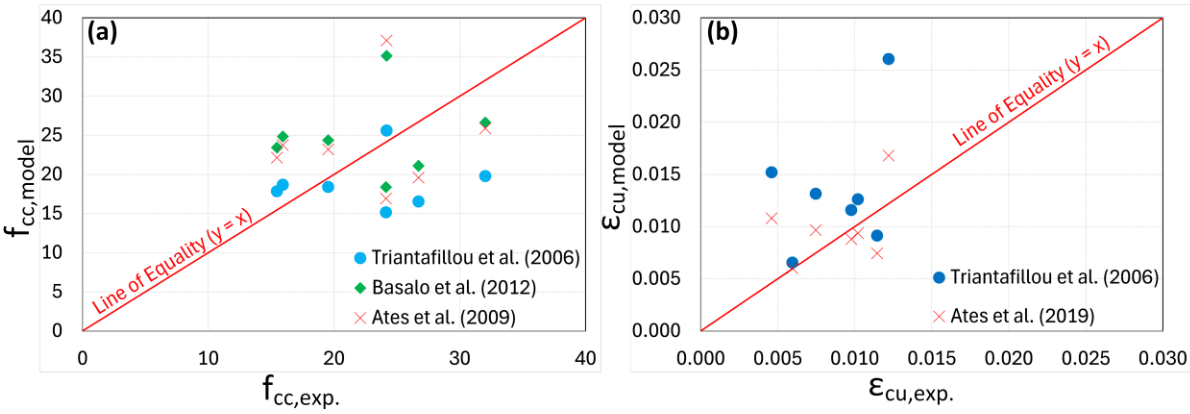

Figure 8. The comparison of the experimental results and model predictions

It should be noted that the proper implementation of the confining layer and assurance of a certain quality in the application of confinement for the method considered in this study is more complicated than those of FRP and even FRCM confinement. The accuracy of the model predictions should also be evaluated from this perspective. Nevertheless, in the authors' opinion, any model to predict the ultimate axial state of concrete confined by a thick composite high-performance reinforced concrete layer should depend on the test results of similarly confined specimens. An increase in the number of studies and more experimental results of this type of confinement is required in this respect. In addition, the nonuniform distribution of tangential stresses produced within the thick composite layer, which is related to the applied lateral confining pressure, should be considered while constituting such a model.

6. Conclusions

The behavior under axial loading of low-strength concrete columns retrofitted with fiber-reinforced mortar and mesh-reinforced jackets was investigated experimentally. By focusing on jacket thickness, fiber properties, and mesh configuration, this study identified the critical performance factors for seismic strengthening. The following conclusions highlight the effectiveness of the proposed method and provide guidance for its future applications.

1. Regardless of the specific test parameters, the proposed jacketing method provided sufficient confinement pressure, leading to varying degrees of axial compressive strength and energy dissipation (i.e., axial strain) capacity improvement in low-quality concrete.
2. The variability in the results and failure to achieve desired improvements in the behavior under axial loading in specific groups can be attributed to application difficulties. Although a superplasticizer was used to ensure good workability in the production of high-strength mortar for jacketing, placing the fiber-reinforced concrete into gaps of 25 mm and especially 15 mm was quite challenging. The use of mesh reinforcement within the layer to provide support further exacerbates this difficulty. Owing to these challenges, voids were observed in the jacketing concrete after demolding certain specimens. These voids were subsequently filled with high-

strength repair mortar and tested in some specimens, as stated previously. However, it was noted that an increase in the repaired area of the specimen negatively impacted the effectiveness of confinement. Furthermore, ensuring a perfectly uniform thickness of the confining layer and precise concentric placement of the mesh reinforcement remained a challenge under laboratory conditions. Potential localized weaknesses or minor misalignments during the casting process may have influenced the consistency of the axial strength results, particularly in specimens where the expected enhancement was not fully realized. These findings highlight the necessity of precise execution and suggest that alternative techniques, such as shotcrete or the use of mortars with even higher workability, could mitigate such issues in future applications.

3. An increase in the thickness of the jacketing mortar layer consistently improved the axial compressive strength. However, a proportional enhancement in the axial strain capacity was not observed in all cases as the mortar thickness increased.
4. An increase in the number of mesh reinforcement layers led to an observed enhancement in energy dissipation and post-elastic strain capacity. The specimens strengthened with two layers of mesh reinforcement demonstrated an improvement exceeding 100% in energy dissipation capacity compared to those strengthened with a single layer. However, a corresponding increase in axial strength was not observed.
5. Groups in which the specimens were confined with a polypropylene fiber-reinforced mortar layer generally exhibited more favorable axial compressive strength than equivalent groups containing steel fibers. Furthermore, post-test observations of the polypropylene fiber-reinforced specimens indicated smaller crack widths than those of their steel fiber-reinforced counterparts.
6. The lateral strains in the confined specimens were measured using two strain gauges positioned equidistantly on a hypothetical circle at the mid-height of the specimen. The results from these strain gauges revealed that the lateral strains varied significantly in magnitude within the same horizontal plane. As expected, the ultimate lateral strains were higher at locations where cracks formed. Similarly, in the FRP-confined concrete test results, the strain gauges over the cracks consistently yielded larger ultimate lateral strains (rupture strains). However, the differences in the values obtained from the strain gauges at different points on the same circle in FRP-confined concrete tests were not of the same magnitude as those observed in the current study (they were much closer). This suggests that the tangential lateral stresses in FRP confinement exhibit a more uniform distribution, which cannot be achieved when a thick mortar layer, as used in the current study, is employed. This leads to the conclusion that, unlike FRP-confined concrete models based on the assumption of uniform lateral stress, modeling the behavior under axial loading of concrete confined with a thick mortar layer necessitates different assumptions. Additionally, although a correlation exists between the axial strength and strain enhancements and lateral rupture strain in FRP-confined concrete, this correlation was not observed in the current study. Further experimental investigations are required to better understand the behavior of modeling the axial response of concrete confined with a thick, fiber-reinforced, mesh-supported mortar layer.
7. The models that depend on the FRP or FRCM-confined concrete test results were considerably scattered compared with the experimental results of this study. In connection with the discussion in the previous conclusion, any confinement model to represent concrete confined by a thick composite concrete layer should be generated using the results of the specimens strengthened using the same methodology.
8. The strengthened specimens could not be evaluated with respect to the position of the mesh reinforcement. This was because the space between the core concrete and the formwork, as mentioned in the previous section, was insufficient to maintain the intended position of the mesh reinforcement. In future studies, as previously suggested, a slightly wider strengthening area should be planned to allow for the assessment of reinforcement placement.
9. The experimental results regarding the influence of mesh reinforcement indicated nuanced behavior. Although the mesh contribution to the ultimate axial compressive strength was not uniformly consistent across all specimens, its impact was more pronounced in the post-peak region. Specifically, the mesh reinforcement enhanced the confinement efficiency by maintaining the integrity of the outer mortar layer even after initial cracking, thereby improving the energy dissipation capacity and leading to more ductile failure modes. The observed inconsistency in the strength enhancement suggests that the primary role of the mesh in this configuration is to

provide lateral stability and prevent premature spalling rather than significantly increasing the peak load-carrying capacity.

Acknowledgements / Funding

This study was supported by the Mersin University Scientific Research Projects Coordination Unit under Project No. 2023-1-TP24841.

Congress and Thesis Statement

This study was presented orally at the 9th National Workshop on Structural Mechanics Laboratories held in Düzce on 18-19 October 2024.
This study was produced from Zeynep UTMA's MSc thesis.

Declaration of Authors' Contribution

Zeynep UTMA: Resource/Material Supply, Data Analysis, Drafting, Revision and Editing; **Emre AKIN:** Control/Observation/Consultancy, Validation, Project Management; **İsmet VAPUR:** Experiment/Observation.

Conflict of Interest Declaration

The authors declare no competing interests.

Declaration of Research and Publication Ethics

The authors declare that they obey the research and publication ethics:
YÖK Scientific Research and Ethics Regulation (yok.gov.tr), Declaration of Helsinki, Commitee on Publication Ethics (COPE), WAME.

Ethics Committee Declaration

The authors declare that the materials and methods used in the article do not require ethics committee approval and/or special legal permission.

Statement on the Use of Artificial Intelligence

The authors declare that they did not use any type of generative artificial intelligence in the writing of this article or in the creation of images, graphics, tables, or their corresponding captions.

References

Akin, E., Tunaboyu, O., & Avsar, O. (2020). Axial behavior of FRP confined low-strength concrete with polyurea. *Structures*, 28, 1774–1784. https://doi.org/10.1016/j.istruc.2020.10.015

Arslan, M. H., & Korkmaz, H. H. (2007). What is to be learned from damage and failure of reinforced concrete structures during recent earthquakes in Turkey? *Engineering Failure Analysis*, 14(1), 1–22. https://doi.org/10.1016/j.engfailanal.2006.01.003

Ates, A. O., Khoshkholghi, S., Tore, E., Marasli, M., & Ilki, A. (2019). Sprayed glass fiber–reinforced mortar with or without basalt textile reinforcement for jacketing of low-strength concrete prisms. *Journal of Composites for Construction*, 23(2), 04019003. https://doi.org/10.1061/(ASCE)CC.1943-5614.0000922

Berthet, J. F., Ferrier, E., & Hamelin, P. (2005). Compressive behavior of concrete externally confined by composite jackets. Part A: Experimental study. *Construction and Building Materials*, 19(3), 223–232. https://doi.org/10.1016/j.conbuildmat.2004.05.012

Carrillo, J., Valencia-Mina, W., & Bojórquez, E. (2020). Compressive performance of square and low-strength concrete columns retrofitted with externally-bonded CFRP. *Materials Today Communications*, 23, 100874. https://doi.org/10.1016/j.mtcomm.2019.100874

Cascardi, A., Aiello, M. A., & Triantafillou, T. C. (2017). Analysis-oriented model for concrete and masonry confined with fiber reinforced mortar. *Materials and Structures, 50*(4), Article 228. https://doi.org/10.1617/s11527-017-1072-0

Colajanni, P., De Domenico, F., Recupero, A., & Spinella, N. (2014). Concrete columns confined with fibre reinforced cementitious mortars: Experimentation and modelling. *Construction and Building Materials*, 52. https://doi.org/10.1016/j.conbuildmat.2013.11.048

De Caso, F. J., Matta, F., & Nanni, A. (2012). Fiber reinforced cement-based composite system for concrete confinement. *Construction and Building Materials*, 32, 55–65. https://doi.org/10.1016/j.conbuildmat.2010.12.063

Donnini, J., Spagnuolo, S., & Corinaldesi, V. (2019). A comparison between the use of FRP, FRCM and HPM for concrete confinement. *Composites Part B: Engineering*, 160, 586–594. https://doi.org/10.1016/j.compositesb.2018.12.111

Ersoy, U. (2009). Seismic rehabilitation of reinforced concrete buildings. In: Tankut, A.T. (eds) *Earthquakes and Tsunamis, Geotechnical, Geological and Earthquake Engineering*, 11, (pp. 7–20). https://doi.org/10.1007/978-90-481-2399-5_2

Ersoy, U., & Özcebe, G. (2000). Lessons from recent earthquakes in Turkey and seismic rehabilitation of buildings. In *S.M. Uzumeri Symposium: Behavior and Design of Concrete Structures for Seismic Performance* (ACI SP-197). American Concrete Institute. https://doi.org/10.14359/11929

Gündoğay, A. (2022). Kentsel dönüşümde iş sağlığı ve güvenliği. *Avrupa Bilim ve Teknoloji Dergisi*, (34), 336–343. https://doi.org/10.31590/ejosat.1068832

Gündoğay, A. (2024). Lifli polimer ile sargılanan betonarme kolonların gerilme-şekil değiştirme ilişkisinin anfis yöntemi ile elde edilmesi. *Journal of Innovations in Civil Engineering and Technology*, *6*(2), 111–130. https://doi.org/10.59314/jicet.1481065

Ilki, A., Kumbasar, N., & Koç, V. (2004). Low strength concrete members externally confined with FRP sheets. Structural Engineering and Mechanics, 18(2), 167–194. https://doi.org/10.12989/sem.2004.18.2.167

Ku, H., Wang, H., Pattarachaiyakoop, N., & Trada, M. (2011). A review on the tensile properties of natural fiber reinforced polymer composites. *Composites Part B: Engineering*, 42(4), 856–873. https://doi.org/10.1016/j.compositesb.2011.01.010

Lam, L., & Teng, J. G. (2003). Design-oriented stress-strain model for FRP-confined concrete. *Construction and Building Materials*, 17(6–7), 471–489. https://doi.org/10.1016/S0950-0618(03)00045-X

Lam, L., Teng, J. G., Cheung, C. H., & Xiao, Y. (2006). FRP-confined concrete under axial cyclic compression. *Cement and Concrete Composites*, 28(10), 949–958. https://doi.org/10.1016/j.cemconcomp.2006.07.007

Mandal, S., Hoskin, A., & Fam, A. (2005). Influence of concrete strength on confinement effectiveness of fiber-reinforced polymer circular jackets. *ACI Structural Journal*, 102(3), 383–392. https://doi.org/10.14359/14409

Mirmiran, A., & Shahawy, M. (1997). Behavior of concrete columns confined by fiber composites. *Journal of Structural Engineering*, 123(5). https://doi.org/10.1061/(ASCE)0733-9445(1997)123:5(583)

Ombres, L., & Mazzuca, S. (2017). Confined concrete elements with cement-based composites: Confinement effectiveness and prediction models. *Journal of Composites for Construction*, 21(3), 04016103. https://doi.org/10.1061/(ASCE)CC.1943-5614.0000755

Ozbakkaloglu, T., & Akin, E. (2012). Behavior of FRP-confined normal- and high-strength concrete under cyclic axial compression. *Journal of Composites for Construction*, 16(4), (pp. 451–463). https://doi.org/10.1061/(ASCE)CC.1943-5614.0000273

Ozbakkaloglu, T., & Oehlers, D. J. (2008). Manufacture and testing of a novel FRP tube confinement system. *Engineering Structures*, 30(9), 2448–2459. https://doi.org/10.1016/j.engstruct.2008.01.014

Ozcan, O., Binici, B., & Özcebe, G. (2010). Yetersiz betonarme kolonlar için lifli polimer güçlendirme tasarım kurallarının irdelenmesi. *Teknik Dergi, 21*(104), 5219–5239.

Özcebe, G., Ersoy, U., Tankut, T., Akyüz, U., & Erduran, E. (2004, August 1–6). *Rehabilitation of existing reinforced concrete structures using CFRP fabrics* [Conference paper]. 13th World Conference on Earthquake Engineering, Vancouver, Canada.

Popov, E. P. (1998). *Engineering mechanics of solids* (2nd ed.). Prentice Hall.

Rousakis, T. C., Karabinis, A. I., & Kiousis, P. D. (2007). FRP-confined concrete members: Axial compression experiments and plasticity modelling. *Engineering Structures*, *29*(7), 1343–1353. https://doi.org/10.1016/j.engstruct.2006.08.006

Song, P. S., & Hwang, S. (2004). Mechanical properties of high-strength steel fiber-reinforced concrete. *Construction and Building Materials*, 18(9). https://doi.org/10.1016/j.conbuildmat.2004.04.027

Tian, H., Zhou, Z., Zhang, Y., & Wei, Y. (2020). Axial behavior of reinforced concrete column with ultra-high performance concrete stay-in-place formwork. *Engineering Structures*, 210, 110403. https://doi.org/10.1016/j.engstruct.2020.110403

Trapko, T. (2013). Fibre reinforced cementitious matrix confined concrete elements. *Materials & Design*, 44. https://doi.org/10.1016/j.matdes.2012.08.024

Triantafillou, T. C., Papanicolaou, C. G., Zissimopoulos, P., & Laourdekis, T. (2006). Concrete confinement with textile-reinforced mortar jackets. *ACI Structural Journal*, 103(1), 28–37.

Üzümeri, Ş. M., Tankut, T., Özcebe, G., & Atımtay, E. (1999). Assessment, repair/strengthening of moderately damaged reinforced concrete buildings in Ceyhan earthquake (1998). In *Uğur Ersoy Symposium on Structural Engineering*. Springer. https://doi.org/10.1007/978-90-481-2681-1_8

Wang, W., Sheikh, M. N., & Hadi, M. N. S. (2016). Axial compressive behaviour of concrete confined with polymer grid. *Materials and Structures,* 49, 3893–3908. https://doi.org/10.1617/s11527-015-0761-9

Wei, Y. Y., & Wu, Y. F. (2012). Unified stress-strain model of concrete for FRP-confined columns. *Construction and Building Materials*, 26(1), 381–392. https://doi.org/10.1016/j.conbuildmat.2011.06.037

Wu, Z., Zhang, J., Yu, H., Wu, Q., & Da, B. (2023). Computer-aided investigation of the tensile behavior of concrete: Relationship between direct and splitting tensile strength. *Structures*, 55. https://doi.org/10.1016/j.istruc.2023.06.019

Zeng, J., & Long, T. (2022). Compressive behavior of FRP grid-reinforced UHPC tubular columns. *Polymers*, 14(1), 125. https://doi.org/10.3390/polym14010125

Zhao, H. (2020). Axial compressive behaviour of concrete strengthened with steel rings, wire mesh and modified high strength mortar (MHSM). *Construction and Building Materials*, 250, 118938. https://doi.org/10.1016/j.conbuildmat.2020.118938